Available online at www.sciencedirect.com
ScienceDirect
Ceramics International 38 (2012) 511–516
CERAMICS INTERNATIONAL
www.elsevier.com/locate/ceramint

Effects of magnesia addition on structural, morphological and magnetic properties of nano-crystalline nickel ferrite system

N.M. Deraz *

Catalytic Chemistry Research Chair, Chemistry Department, College of Science, King Saud University, Riyadh, Saudi Arabia

Received 13 June 2011; received in revised form 15 June 2011; accepted 17 July 2011
Available online 26th July 2011

Abstract

Nano-crystalline magnesia doped nickel ferrite powders have been synthesized by the combustion route. The structural, morphological and magnetic properties of the products were determined by X-ray diffraction (XRD), scanning electron microscopy (SEM), energy-dispersive X-ray (EDX) spectroscopy and vibrating sample magnetometer (VSM). X-ray analysis showed that all samples were cubic spinel. The increase in magnesia concentration resulted in a decrease in the average crystallite size, lattice constant, unit cell volume, X-ray density, ionic radii, the distance between the magnetic ions and bond lengths on tetrahedral sites and octahedral sites of the as prepared ferrite. The combustion method led to formation of spongy and fragile network structure. Increasing amounts of magnesia brought about remarkable changes in the microstructure and porosity of nickel ferrite. Doping of nickel ferrite by magnesia led to a decrease in its saturation magnetization. The minimum saturation magnetization value of nickel ferrite due to the doping 1 wt.% MgO attained 44.18 emu/g.

Keywords: XRD; SEM; EDX; VSM; $NiFe_2O_4$; MgO doping

1. Introduction

In recent years, we have seen a significant growth in the study of nano-materials such as nano-crystalline ferrite. These ferrites have attracted much attention due to their surface and quantum confinement effects depending upon large surface-to-volume ratio and size-dependent properties, respectively. These parameters resulted in different modifications in the physical and chemical properties of ferrites [1,2]. So, ferrite based nano-materials are different from their bulk counterparts.

Synthesis of nano-crystalline ferrite through different routes has become an essential part of research and development in order to obtain materials with the desired physical and chemical properties. Various chemical and physical methods including chemical co-precipitation, high energy milling, hydrothermal processing, sol–gel and mechanical mixing method have been attempted to produce nano-crystalline ferrites [3–10]. These techniques have some disadvantages such as complex processes, expensive precursors and low production rates [11]. Recently, a solution combustion method has been utilized to synthesize simple and mixed metal oxides at a lower temperature in a surprisingly short time. This quick, straightforward process can be used to synthesize homogeneous, high-purity, crystalline oxide ceramic powders including ultrafine ferrite composites with a broad range of particle sizes [12–18].

Among the different spinel ferrites, nickel ferrites ($NiFe_2O_4$) are the most versatile magnetic materials for general use in microwave devices, power transformers in electronics, rod antennas, read/write heads for high speed digital tape, and gas sensing material [19–21]. Ni-ferrite is an inverse spinel in which half of the Fe^{3+} ions preferentially fill the A sites and the rest occupy the B sites. Thus, $NiFe_2O_4$ can be represented by the formula $(Fe^{3+})_A[Ni^{2+}Fe^{3+}]_BO_4^{2-}$ [15]. Nano-crystalline $NiFe_2O_4$ were synthesized by a simple and cost-effective route using Ni and Fe nitrates and glycine. Size-controlled nickel ferrite nano-particles were successfully synthesized via glycine–nitrate method using different amounts of glycine. The increase in ratio between glycine and nitrates led to an increase in crystalline phase, crystallite size, and particle size, lattice constant and magnetic properties of the nano-crystalline nickel ferrite [15]. Doping process

* Tel.: +966 541684405.
E-mail address: nmderaz@yahoo.com.

0272-8842/$36.00
doi:10.1016/j.ceramint.2011.07.036

could drastically affect the physical and chemical properties of different ferrites [22]. Sertkol et al. reported that synthesize nanocrystalline Zn-doped nickel ferrite from a stoichiometric mixture of corresponding metal nitrates and urea powders. Magnetic properties showed anomalities as the Zn doping level increased. This has been explained and attributed to the relative positions of Ni, Zn, and Fe ions in the crystal lattice [23]. Mishra et al. studied the effect of niobium-doping on the structural, electrical and magnetic properties of nickel ferrite. These authors found that doping of nickel ferrite with niobium ion led to decrease in both their size and magnetization with an increase in the coercive field. This behavior can be explained introducing core–shell model of magnetic nano-particles [24].

Little research work has been conducted to investigate the effect of Mg ion on the physical properties of nano-metric Ni ferrite. One decided to examine the influence of MgO-doping on the magnetic properties of Ni ferrite nano-particles to open new area of applications for such ferrite. In this context, the goal of this paper is to prepare pure and magnesia doped $NiFe_2O_4$ nano-particles. Our contribution to the area of magnetism just outlined is to investigate the relationship between preparation route, MgO-doping, structure and properties of the as prepared ferrite. Our ultimate goal is to understand the influence of doping process using magnesia on the cation distribution of doped nickel ferrites. The techniques employed were XRD, EDX, SEM and VSM.

2. Experimental

2.1. Materials

Undoped and MgO-doped $NiFe_2O_4$ samples were prepared by mixing calculated proportions of nickel and iron nitrates with glycine in presence of different amounts of magnesium nitrate. The mixed precursors were concentrated in a porcelain crucible on a hot plate at 350 °C for 10 min. The crystal water was gradually vaporized during heating and when a crucible temperature was reached, a great deal of foams produced and spark appeared at one corner which spread through the mass, yielding a voluminous and fluffy product in the container. Hence, the as-prepared products were heat treated at 700 °C for 1 h to enhance their crystallinity and remove the residual charred organic materials. In this investigation, the concentrations of magnesium expressed as wt.% MgO were 0.34, 0.68 and 1. The chemicals employed in the present work were of analytical grade supplied by Prolabo Company.

2.2. Characterization of the as synthesized materials

An X-ray measurement of various mixed solids was carried out using a BRUKER D8 advance diffractometer (Germany). The patterns were run with Cu K_α radiation at 40 kV and 40 mA with scanning speed in 2θ of 2° min^{-1}.

The crystallite size of pure and MgO-doped $NiFe_2O_4$ present in the investigated solids was based on X-ray diffraction line broadening and calculated by using Scherrer equation [25].

$$d = \frac{B\lambda}{\beta\cos\theta}$$

where d is the average crystallite size of the phase under investigation, B is the Scherrer constant (0.89), λ is the wave length of X-ray beam used, β is the full-width half maximum (FWHM) of diffraction and θ is the Bragg's angle.

Scanning electron micrographs (SEMs) was recorded on JEOL JAX-840A electron microanalyzer. The samples were dispersed in ethanol and then treated ultrasonically in order to disperse individual particles over gold grids.

Energy dispersive X-ray (EDX) analysis was carried out on Hitachi S-800 electron microscope with an attached kevex Delta system. The parameters were as follows: accelerating voltage 10–20 kV, accumulation time 100 s, and window width 8 μm. The surface molar composition was determined by the Asa method, Zaf-correction, and Gaussian approximation.

2.3. Magnetic properties of the as prepared materials

The magnetic properties of the investigated solids were measured at room temperature using a vibrating sample magnetometer (VSM; 9600-1 LDJ, USA) in a maximum applied field of 15 kOe. From the obtained hysteresis loops, the saturation magnetization (M_s), remanence magnetization (M_r) and coercivity (H_c) were determined.

3. Results and discussion

3.1. XRD analysis

The polycrystalline samples of pure and MgO-doped nickel ferrite have been investigated by X-ray diffraction. The XRD patterns of pure and MgO-doped nickel ferrite solid specimens are shown in Fig. 1. All compositions of pure and MgO-doped nickel ferrite samples could be indexed in terms of a single phase cubic spinel structure. The analysis of the diffraction pattern by using (2 2 0), (3 1 1), (4 0 0), (4 2 2), (5 1 1), (4 4 0), (6 2 0), and (5 3 3) reflection planes confirm the formation of well nano-crystalline $NiFe_2O_4$. An increase in the concentration of magnesia resulted in a measurable decrease in the degree of crystallinity of produced phase depending upon the decrease in the intensity of diffraction peaks of spinel nickel ferrite.

The intensities of (2 2 0) and (4 4 0) planes are more sensitive to the cations on tetrahedral and octahedral, respectively [1,16]. Table 1 shows the observed intensities of the above two planes and the intensity ratio between them. It can be observed that the intensities of the previous planes and the ratio between them decrease with the addition of magnesia indicating to the preference of the Mg^{2+} by the octahedral and tetrahedral sites. Indeed, The decrease in the intensity of the (2 2 0) plane is greater than that of the (4 4 0) plane. This result might show the increasing amounts of Mg^{2+} located on tetrahedral sites due to Mg-doping process.

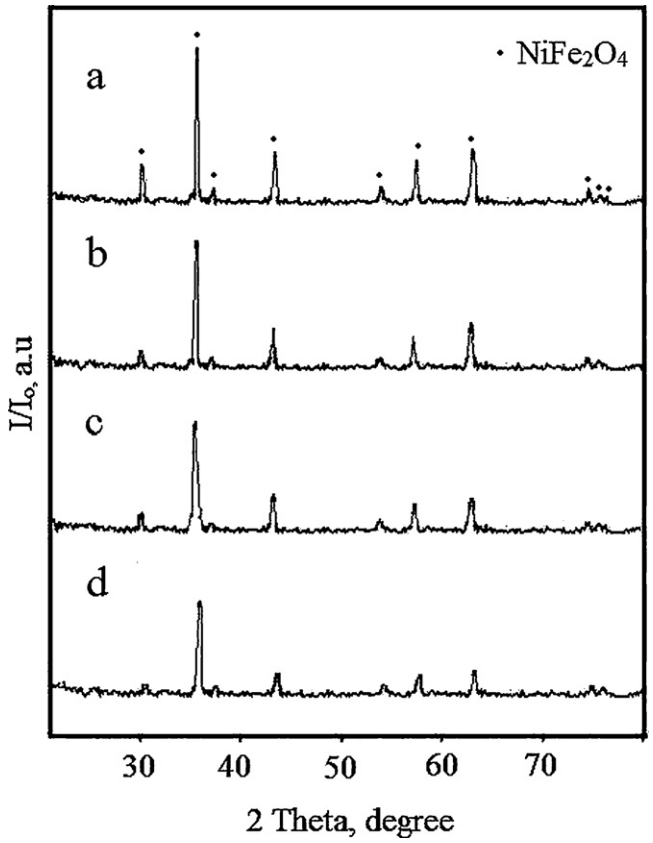

Fig. 1. XRD patterns for pure and Mg-doped samples: (a) 0.00; (b) 0.34; (c) 0.68 and (d) 1 wt.% MgO.

An X-ray data enable us to investigation the role of the magnesia doping process in modifying the structural parameters such as the crystallite size (d), lattice constant (a), unit cell volume (V), X-ray density (D_x), ionic radii (r_A and r_B), the distance between the magnetic ions (L_A and L_B) and bond lengths (A–O and B–O) on tetrahedral (A) sites and octahedral (B) sites of cubic spinel structure for the produced nickel ferrite crystallites. The estimated values of various structural parameters are given in Tables 2 and 3. It can be seen in Table 2 that the rise in the concentration of magnesium species brought about a decrease in the values of crystallite size, lattice constant and unit cell volume of the as synthesized ferrite. Opposite behavior was observed for the value of X-ray density. However, the results in Table 3 shows that the values of L_A, L_B, r_A, r_B, A–O and B–O decrease as the amount of Mg species increases. These findings could be attributed to the incorporation of magnesium ions, having smaller ionic radii, in the lattice of nickel ferrite with subsequent redistribution of cations among octahedral and tetrahedral sites [1,16].

Table 1
The effects of MgO-doping on the intensity values of hkl planes of $NiFe_2O_4$ phase.

Concentration of MgO (wt.%)	Peak height (a.u.)		
	I_{220}	I_{440}	I_{220}/I_{440}
0.00	29.9	44.6	0.666
0.34	25.7	39.8	0.646
0.68	20.8	35.7	0.583
1.00	17.6	30.8	0.571

Table 2
The effects of MgO-doping on some structural parameters of nickel ferrite.

Concentration of MgO (wt.%)	d (nm)	a (nm)	V (nm^{-3})	D_x (g/cm^3)
0.00	62	0.8340	0.5801	5.372
0.34	49	0.8325	0.5770	5.401
0.68	41	0.8320	0.5759	5.411
1.00	38	0.8311	0.5741	5.428

3.2. SEM analysis

The morphology of the pure and nickel ferrite doped with 0.34 and 0.68 wt.% MgO were determined by SEM. SEM images given in Fig. 2a–c of pure and doped nickel ferrite specimens reveal remarkable changes in the microstructure and porosity. One can see the formation of spongy and fragile network structure. The voids and pores present in the samples are attributed to the release of large amount gases during combustion process. The increase in the amount of magnesia brought about an increase in the extent of voids and pores with week agglomeration and fracture surfaces of the powders.

3.3. EDX analysis

Energy dispersive X-ray (EDX) analysis of the pure and nickel ferrite doped with 0.34 and 0.68 wt.% MgO specimens was carried out. The EDX analysis using acceleration voltage set at 10, 15 and 20 keV were performed to determine the chemical composition of the elements present from the surface to the interior of the solids and to confirm the homogeneity of the as prepared samples. Fig. 3a–c displays EDX spectrums of the previous samples at 20 keV. The spectrum of different samples indicated the presence of Fe, Ni, Mg and O as the major elements in the material studied with absence of any impurities.

The relative atomic abundance of Mg, Ni, Fe and oxygen species present in the uppermost surface and bulk layers of various solids are given in Table 4. Also, Table 4 shows the results obtained from the energy-dispersive X-ray analysis at 10–20 keV for the pure and doped nickel ferrite samples. The concentrations of Fe are much lower on the surface with an electron beam at 10 keV than that in the interior of pure samples and those treated with 0.34 wt.% MgO with an electron beam at 20 keV. For these samples, the concentrations of Ni and Mg are much higher on the surface with an electron beam at 10 keV than that in the interior with an electron beam at 20 keV. Opposite behaviors were observed for the sample doped with 0.68 wt.% MgO. The concentration of Fe element at surface and/or interior layers decreases as the amount of magnesium species increases. Opposite behavior was observed for Ni and Mg elements due to increasing amounts of magnesia.

The homogeneity of the samples is determined from the EDX spectrum over a selected zone. The spectrum of each

Table 3
The effects of MgO-doping on the values of L_A, L_B, A–O, B–O, r_A and r_B of cobalt ferrite.

Concentration of MgO (wt.%)	L_A (nm)	L_B (nm)	A–O (nm)	B–O (nm)	r_A (nm)	r_B (nm)
0.00	0.3611	1.1794	0.2022	0.1959	0.0672	0.0609
0.34	0.3605	1.1773	0.2019	0.1956	0.0669	0.0606
0.68	0.3602	1.1766	0.2018	0.1955	0.0667	0.0605
1.00	0.3599	1.1753	0.2015	0.1953	0.0665	0.0603

sample was recorded for three points with an electron beam at 20 keV. The summary of elements (Mg, Ni, Fe and O) distribution is shown in Table 4. It can be seen from this table that the concentrations of these elements are close to each other at the three different points. This observation shows that the previous elements are almost homogeneously distributed over the selected zone of the samples investigated.

3.4. Magnetic study

Magnetic hysteresis loops observed for the Mg-doped nickel ferrite system at room temperature and applied field of 15 kG are shown in Fig. 4. The effects of the change in the concentrations of magnesia on the values of the saturation magnetization (M_s), remanence magnetization (M_r) and coercivity (H_c) and magnetic moment (n_B) of the nickel ferrite are summarized in Table 5. Recently, our previous studies shows that the saturation magnetization of nickel ferrite was 51 emu/g [15]. Investigation of Table 5 reveals that: (i) the increase in the amount of magnesia led to a decrease in the values of saturation magnetization and remanence magnetization of nickel ferrite. The maximum decrease in the value of M_s due to the increase in the amount of magnesia attained 13.37%. (ii) The value of magnetic moment decrease as the concentration of Mg species in doped nickel ferrite increases. The maximum decrease in the value of n_B due to the increase in the amount of Mg species attained 13.37%. (iii) The treatment of nickel ferrite with different amounts of MgO brought about a decrease in the value of H_c. The dissolution of Mg^{2+} ions in the lattices of NiO and Fe_2O_3, involved in the forming nickel ferrite, can proceed via substitution of some host Ni^{2+} and Fe^{3+} ions and/or also by their location in interstitial positions forming solid solution. This dissolution led to re-orientation and contraction of the cations included in the nickel ferrite formation. These findings brought about significant changes in the magnetic properties.

The low magnetic moments due to incorporation of Mg ions in the nickel ferrite lattice can be explained in terms of the

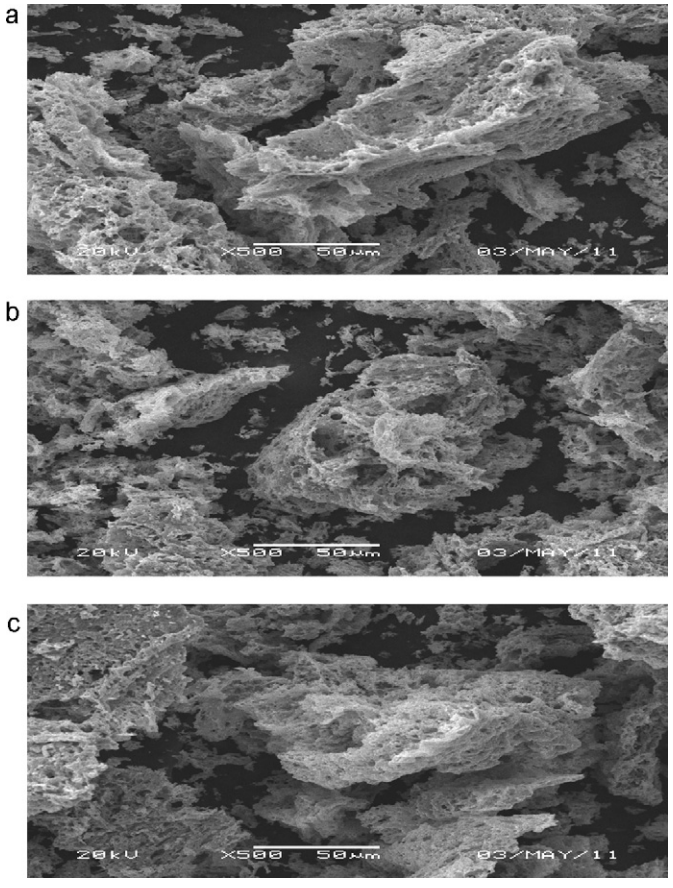

Fig. 2. SEM images for pure and Mg-doped samples: (a) 0.00; (b) 0.34 and (c) 0.68 wt.% MgO.

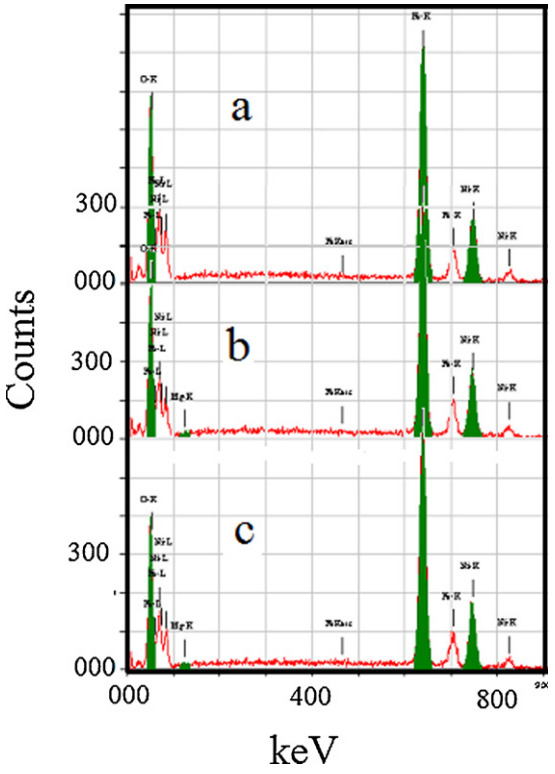

Fig. 3. EDX patterns for pure and Mg-doped samples: (a) 0.00; (b) 0.34 and (c) 0.68 wt.% MgO.

Table 4
The effects of MgO-doping on the atomic abundance of elements involved in the as prepared solids.

Concentration of MgO (wt.%)	Elements	Atomic abundance (%)				
		10 keV	15 keV	20 keV	20 keV	20 keV
0.00	O	13.44	10.12	13.32	18.10	17.20
	Fe	66.78	68.03	61.55	57.26	57.25
	Ni	19.79	21.85	25.13	24.64	25.10
	Mg	00.00	00.00	00.00	00.00	00.00
0.34	O	19.58	16.93	20.66	20.97	16.06
	Fe	59.53	57.25	52.88	53.32	58.05
	Ni	21.10	25.81	26.42	25.63	25.51
	Mg	00.00	00.00	0.04	0.08	0.39
0.68	O	14.69	13.54	16.62	21.02	14.73
	Fe	53.87	63.01	58.94	53.21	60.64
	Ni	30.98	23.33	24.23	25.60	24.36
	Mg	0.46	0.12	0.21	0.16	0.27

non-collinear spin arrangement, i.e., the presence of a small canting of the B site moment with respect to the direction of the A site moment [26,27]. Then, the B–O–B coupling interaction between magnetic ions at the B sublattice becomes stronger than the A–O–B coupling interaction between magnetic ions at the A and B sublattices, which leads to the existence of randomly canted structure at B site and forms triangular configuration in the ferrite system. As a result, the transition from the collinear parallel arrangement to non-parallel for the magnetic moments of the Fe cations at B site causes the reduction of the saturated magnetization. Therefore, it can be reasonably concluded that at high substitution level the falling of the magnetization is originated from the stronger B–O–B super-exchange interaction.

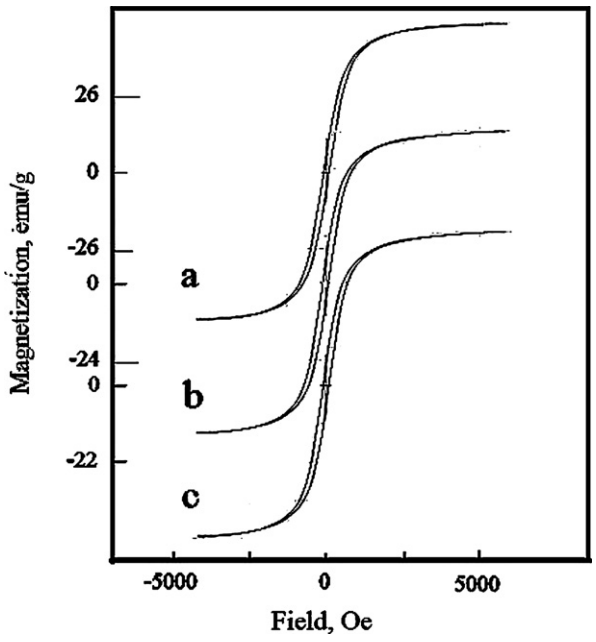

Fig. 4. Magnetic hysteresis curves measured at a room temperature for Mg-doped samples: (a) 0.34; (b) 0.68 and (c) 1 wt.% MgO.

Table 5
The effects of MgO-doping on the magnetic properties (M_s, M_r and H_c) of the as-prepared solids.

Concentration of MgO (wt.%)	M_s (emu/g)	M_r (emu/g)	M_r/M_s (emu/g)	H_c (Oe)	n_B
0.00[a]	51.00	15.51	0.303	118.30	2.142
0.34	51.53	13.98	0.271	92.46	2.164
0.68	47.78	13.81	0.289	98.64	2.007
1.00	44.18	13.07	0.296	97.36	1.856

[a]All magnetic parameters for pure nickel ferrite indexed in our previous work [15].

4. Conclusions

Nano-crystalline pure and magnesia doped nickel ferrite can be prepared by the combustion method for the full range of composition. The structural, morphology and magnetic properties of the obtained materials have been studied. The formation of single s cubic phase $NiFe_2O_4$ was confirmed by the XRD technique. SEM and EDX measurements showed the chemical composition, elements distribution and homogeneity of the as prepared solids. The lattice constant, unit cell volume, ionic radii, the distance between the magnetic ions and bond lengths on tetrahedral sites and octahedral sites of cubic spinel structure were found to decrease with the increase in magnesia concentration. The average crystallite size decreases as the concentration of Mg species increases. The saturation magnetization was found to decrease with the increase in magnesia content. However, low coercivity was observed for the Mg-doped nickel ferrite nano-particles. The high quality of th as prepared materials, especially their homogeneity, nano-crystallinity and saturation magnetization, suggests that combustion method using glycine is a promising route for preparing pure and magnesia doped nickel ferrite nano-particles which can be used for many practical applications.

Acknowledgement

This project was supported by King Saud University, Deanship of Scientific Research, College of Science Research Centre.

References

[1] N.M. Deraz, Glycine-assisted fabrication of nanocrystalline cobalt ferrite system, J. Anal. Appl. Pyrol. 88 (2010) 103.

[2] N.M. Deraz, Size and crystallinity-dependent magnetic properties of copper ferrite nano-particles, J. Alloys Compd. 501 (2010) 317.

[3] M. Jalaly, M.H. Enayati, F. Karimzadeh, Investigation of structural and magnetic properties of nano-crystalline $Ni_{0.3}Zn_{0.7}Fe_2O_4$ prepared by high energy ball milling, J. Alloys Compd. 480 (2009) 737.

[4] F. Gozuak, Y. Koseoğlu, A. Baykal, H. Kavas, Synthesis and characterization of $Co_xZn_{1-x}Fe_2O_4$ magnetic nano-particles via a PEG-assisted route, J. Magn. Magn. Mater. 321 (2009) 2170.

[5] T. Ozkaya, M.S. Toprak, A. Baykal, H. Kavas, Y. Koseoğlu, B. Aktas, Synthesis of Fe_3O_4 nanoparticles at 100 °C and its magnetic characterization, J. Alloys Compd. 472 (2009) 18.

[6] A. Angermann, J. Töpfe, Synthesis of nanocrystalline Mn–Zn ferrite powders through thermolysis of mixed oxalates, Ceram. Int. 37 (3) (2011) 995.

[7] M.S. Toprak, B.J. McKenna, M. Mikhaylova, J.H. Waite, G.D. Stucky, Spontaneous assembly of magnetic microspheres, Adv. Mater. 19 (2007) 1362.

[8] S. Li, J. Qin, A. Fornara, M.S. Toprak, M. Muhammed, D.K. Kim, Synthesis and magnetic properties of bulk transparent PMMA/Fe-oxide nanocomposites, Nanotechnology 20 (2009) 185607.

[9] N.M. Deraz, M. Hessian, Structural and magnetic properties of pure and doped nano-crystalline cadmium ferrite, J. Alloys Compd. 475 (2009) 832.

[10] N.M. Deraz, Production and characterization of pure and doped copper ferrite nano-particles, J. Anal. Appl. Pyrol. 82 (2) (2008) 212.

[11] Z. Yue, J. Zhou, L. Li, H. Zhang, Z. Gui, Synthesis of nano-crystalline NiCuZn ferrite powders by sol–gel auto-combustion method, J. Magn. Magn. Mater. 208 (2000) 55.

[12] Y.P. Fu, C.H. Lin, Microwave-induced combustion synthesis of Ni–Zn ferrite powder and its characterization, J. Magn. Magn. Mater. 251 (2002) 74.

[13] A.C.F.M. Costa, E. Tortella, M.R. Morelli, R.H.G.A. Kiminami, Synthesis, microstructure and magnetic properties of Ni–Zn ferrites, J. Magn. Magn. Mater. 256 (2003) 174.

[14] N.M. Deraz, S. Shaban, Optimization of catalytic, surface and magnetic properties of nano-crystalline manganese ferrite, J. Anal. Appl. Pyrol. 86 (2009) 173.

[15] A. Alarifi, N.M. Deraz, S. Shaban, Structural, morphological and magnetic properties of $NiFe_2O_4$ nanoparticles, J. Alloys Compd. 486 (2009) 501.

[16] N.M. Deraz, A. Alarifi, Synthesis and characterization of pure and Li_2O doped $ZnFe_2O_4$ nanoparticles via glycine assisted route, Polyhedron 28 (2009) 4122.

[17] N.M. Deraz, M.K. El- Aiashy, Suzan A. Ali, Structural, surface and catalytic properties of nanosized ceria catalysts, Adsorpt. Sci. Technol. 27 (2009) 803.

[18] N.M. Deraz, Fabrication and characterization of magnetic alumina-doped zinc ferrite nanoparticles, J. Anal. Appl. Pyrol. 91 (2011) 48.

[19] A.C.F.M. Costa, V.J. Silva, D.R. Cornejo, M.R. Morelli, R.H.G.A. Kiminami, L. Gama, Magnetic and structural properties of $NiFe_2O_4$ ferrite nano-powder doped with Zn^{2+}, J. Magn. Magn. Mater. 320 (2008) e370.

[20] V.D. Kapse, S.A. Ghosh, F.C. Raghuwanshi, S.D. Kapse, Nanocrystalline spinel $Ni_{0.6}Zn_{0.4}Fe_2O_4$: a novel material for H_2S sensing, Mater. Chem. Phys. 113 (2009) 638.

[21] V.D. Kapse, S.A. Ghosh, F.C. Raghuwanshi, S.D. Kapse, U.S. Khandekar, Nanocrystalline $Ni_{0.6}Zn_{0.4}Fe_2O_4$: a novel semiconducting material for ethanol detection, Talanta 78 (2009) 19.

[22] E. Rezlescu, N. Rezlescu, P.D. Popa, L. Rezlescu, C. Pasnicu, M.L. Craus, Effect of copper oxide content on intrinsic properties of MgCuZn ferrite, Mater. Res. Bull. 33 (6) (1998) 915.

[23] M. Sertkol, Y. Koseoğlu, A. Baykal, H. Kavas, A. Bozkurt, M.S. Toprak, Microwave synthesis and characterization of Zn-doped nickel ferrite nanoparticles, J. Alloys Compd. 486 (2009) 325.

[24] S. Mishra, N. Karak, T.K. Kundu, D. Das, N. Maity, D. Chakravorty, Nanocrystalline nickel ferrites prepared by doping with niobium ions, Mater. Lett. 60 (2006) 1111.

[25] B.D. Cullity, Elements of X-Ray Diffraction, Addison-Wesley Publishing Co. Inc, 1976 (Chapter 14).

[26] F. Li, H. Wang, L. Wang, J. Wang, Magnetic properties of $ZnFe_2O_4$ nanoparticles produced by a low-temperature solid-state reaction method, J. Magn. Magn. Mater. 309 (2007) 295.

[27] Y. Koseoğlu, H. Kavas, Size and surface effects on magnetic properties of Fe_3O_4 nano-particles, J. Nanosci. Nanotechnol. 8 (2008) 584.